UNIVERSIDAD NACIONAL DE COLOMBIA
SEDE MEDELLÍN
FACULTAD DE MINAS

DYNA
http://dyna.medellin.unal.edu.co/

Lattice-Boltzmann method applied to the pattern formation on periodic surface structures generated by multiline nanosecond laser

Frank Rodolfo Fonseca-Fonseca [a], José Edgar Alfonso-Orjuela [b] & Darío Fernando Andrade [c]

[a] *Departamento de Física, Universidad Nacional de Colombia, Colombia. frfonsecaf@unal.edu.co*
[b] *Departamento de Física, Universidad Nacional de Colombia. Colombia. jealfonsoo@unal.edu.co*
[c] *Grupo de Ciencia de Materiales y Superficies, Universidad Nacional de Colombia, Colombia.* dfandradez@hotmail.com

Received: August 9th, 2013. Received in revised form: June 3th, 2014. Accepted: July 9th, 2014.

Abstract
We simulated the pattern formation on silicon surfaces. For this purpose, we used Lattice-Boltzmann method assuming two non-ideal interacting fluids using a lattice velocity D2Q9. The experiment was carried out with a multiline (1064, 532 and 355 nm) Nd: YAG pulsed laser that employs an energy range from 310 to 3100 J on a surface p-type monocrystalline silicon oriented in the direction [111]. The whole system was subjected to argon gas blowing which is key in pattern formation. Computer simulation reproduces the overall behavior of the experimental geometric patterns expressed in oblique parallel ripples quite well.

Keywords: Laser Ablation, monocrystalline, non-ideal fluids, Lattice-Boltzmann method.

Método de Lattice-Boltzmann aplicado a la formación de patrones sobre estructuras superficiales periódicas generadas por láser de nanosegundos multilineas

Resumen
Hemos simulado la formación de patrones en superficies de silicio. Para este propósito, se utilizó el método de Lattice-Boltzmann suponiendo dos fluidos no ideales, que interactúan, utilizando una rejilla de velocidades ***D2Q9***. El experimento se llevó a cabo con un láser de pulsos multilínea (1064, 532 y 355 nm) de Nd: YAG, que emplea un rango de energía 310 a 3.100 J, en una superficie de silicio monocristalino, tipo p, orientado en la dirección [111]. Todo el sistema se sometió a soplado de gas de argón que es clave en la formación de los patrones. La simulación computacional reproduce bastante bien, el comportamiento global de los patrones geométricos experimentales, expresados en ondulaciones paralelas oblicuas.

Palabras clave: Ablación Láser, monocristalino, Fluidos no ideales, método de Lattice-Boltzmann.

1. Introduction

The Lattice-Boltzmann method (LBM) has become one of the most popular techniques for studying the phenomenology of complex fluid dynamics in recent decades. This technique [1-3], is based on the discretization of the Boltzmann equation with Bathnagar, Groos y Krook (BGK) approximation [4] for the collision operator. In LBM, the statistical distribution of particles $f_i(x,t)$, is located on a spatial grid, where each spatial point is assigned to a discrete and finite set of velocity vectors e_i, $i = 1,\ldots,n_d$, which point to the nearest sites. LBM solves a discrete kinetic equation for one particle distribution function $f_i(x,t)$, along the above discrete set of velocities. For carrying out a LBM, a discrete velocity e_i is chosen, in one-dimension D1Q3 and (D1Q5 are common. In two dimensions D2Q9 is well-known for 2D simulations and in 3D we have the D3Q15, D3Q27 and D3Q19 lattices.

A wide range of simulations has used these lattices up to now. Among them we can find simulation of ferrofluids [5], a competition between surface tension and dipolar interactions to model magnetic fluids [6], and the simulation of electroosmotic fluids in charged anisotropic porous material [7]. Using a higher moment method, it is also possible to give rise to the Kortweg-De Vries equation [8], and furthermore LBM has been used to simulate incompressible magnetohydrodynamics

in two or three dimensions [9]. Likewise, the application of LBM to the calculation of the ground state of Gross-Pitaevskii equation corresponding to the derivation of a quantum mechanical analysis is current [10]. Furthermore, using suitable boundary conditions, the effect of wettability on solid-fluid interfaces has been investigated, and also there have been studies of the effect of the influence of viscous coupling on two-phase flow applied to porous media [11]. Shan & Chen [12] presented an LBM model that is able to simulate flows of multiple phases, and Luo [13] developed a model based on the discretized Boltzmann equation for the two fluid phases.

On the other hand, laser-matter interaction and the generation of surface periodic structures is a very important research area with enormous technological applications. In general, the surface periodicity can be understood as interference between the incident laser beam and the scattered beam parallel to the substrate [14]. Indeed, it is possible to add other physical effects such as surface waves attributed to roughness and in-homogeneities, etc. [15]. Further, dielectric materials such as semiconductor surfaces have been used to produce periodic structures using femtosecond and picosecond lasers [16]. For silicon, which is an indirect band gap semiconductor material, low electro-optic efficiency limits its use. Some responses can be enhanced by modifying its surface by using different techniques, which involve the manipulation of the surface by changing the process parameters such as the treatment atmosphere, the energy density and the initial state of the material's surface, [17,18]. In general, morphological and structural changes on the surface of a material can produce changes in its optical, electrical and mechanical properties, which can potentially improve the performance of components made of such material [19,20].

This paper deals with periodic surface structures over p-type silicon surfaces using laser irradiation with a multiline (1064, 532, 355 nm) Nd:YAG pulsed laser were obtained. In section 2, we present a short review of the Lattice-Boltzmann method and the equilibrium function based on the D2Q9 lattice scheme velocity is shown. In section 3, we present the potential interaction between particles. Section 4 outlines the experimental setup. Results are given in Section 5 and conclusions in Section 6.

2. The Lattice-Boltzmann Method

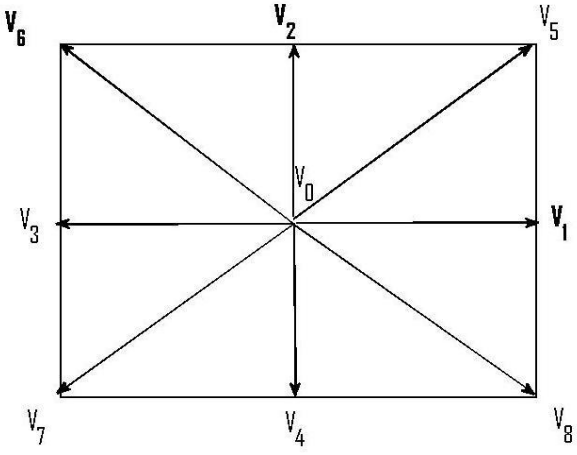

Figure 1. D2Q9 scheme for the velocity lattice. (Figure elaborated in gnuplot [32]).

A summary of the Lattice-Boltzmann method is as follows, [3]. This technique will be applied to the system to reproduce the surface pattern. The Lattice-Boltzmann equation is:

$$f_{i,j}(x + e_x\delta t, t + \delta t) = f_{i.j}(x,t) + \Omega_{i,j}(x,t) \quad (1)$$

In the above expression, $f_{i,j}$ represents the one-particle distribution function, $\Omega_{i,j}$ is the collision operator, which measures the rate of change of $f_{i,j}$ during collision. Both δx and δt represent the spatial and temporal discretization in the system. The density ρ_j and the momentum density $\rho\vec{v}$ are defined as the moments of the distribution function $f_{i,j}$:

$$\rho_j = \sum_i {f^0}_{i,j} \quad (2)$$

$$\rho_j\vec{v} = \sum_i \vec{e}_i {f^0}_{i,j} \quad (3)$$

The collision operator $\Omega_{i,j}(x,t)$, must satisfy the conservation of momentum equation and the total mass on the grid point, so:

$$\sum \Omega_i = 0 \quad (4)$$

$$\sum \Omega_i\vec{e}_i = 0 \quad (5)$$

Doing a Taylor series expansion in space and time, Eq. (1), we obtain:

$$\delta t\left(\frac{\partial}{\partial t} + e_x\frac{\partial}{\partial x_1}\right)f_{i,j} + \frac{\delta t^2}{2}\left(\frac{\partial}{\partial t} + e_x\frac{\partial}{\partial x_1}\right)^2 f_{i,j} = \frac{\Omega_{i,j}}{\varepsilon} \quad (6)$$

Where we have used $\delta x = v_x\delta t$, $\delta y = v_y\delta t$, and $\vec{v}_i \cdot \nabla = e_x\frac{\partial}{\partial x} + e_y\frac{\partial}{\partial y}$. Also a perturbative expansion known as Chapman-Enskog expansion is employed, and the expansion parameter is defined as ε which is the same for the spatial and time derivatives. Therefore:

$$\frac{\partial}{\partial t} = \varepsilon\frac{\partial}{\partial t_1} + \varepsilon^2\frac{\partial}{\partial t_2} \quad (7)$$

$$\frac{\partial}{\partial x} = \varepsilon\frac{\partial}{\partial x_1} \quad (8)$$

$$\frac{\partial}{\partial y} = \varepsilon\frac{\partial}{\partial y_1} \quad (9)$$

Expanding the distribution function $f_{i,j}$ in a perturbative series:

$$f_{i,j} = {f^0}_{i,j} + \varepsilon{f^1}_{i,j} + \varepsilon^2{f^2}_{i,j} \quad (10)$$

Equation (7) assumes that time t_1 is much greater than t_2. Similarly, the distribution function f_i can formally be expanded around the distribution function of statistical equilibrium, as:

$$f_{i,j} = f^{eq}{}_{i,j} + \mathcal{E} f^{neq}{}_{i,j} \quad (11)$$

Where $f^{eq}{}_{i,j} = f^{0}{}_{i,j}$. Moreover, using probability conservation the following conditions are imposed on $f^{eq}{}_{i,j}$:

$$\rho_j = \sum_i f^{eq}{}_{i,j} \quad (12)$$

$$\rho_j \vec{v} = \sum_i \vec{e}_i f^{eq}{}_{i,j} \quad (13)$$

In eq. (11), $f^{neq}{}_{i,j}$ is the distribution function of the statistical non-equilibrium, and can be expanded as:

$$f^{neq}{}_{i,j} = f^{1}{}_{i,j} + \mathcal{E} f^{2}{}_{i,j} \quad (14)$$

And it is subject to the following restrictions. For $k \geq 1$, we have:

$$\sum f^{k}{}_{i,j} = 0 \quad (15)$$

$$\sum f^{k}{}_{i,j} \vec{e}_i = 0 \quad (16)$$

We assume the BGK expansion, [4], for the collision operator Ω_i:

$$\Omega_{i,j}(x,t) = -\frac{1}{\tau}(f_{i,j}(x,t) - f^{eq}{}_{i,j}(x,t)) \quad (17)$$

Where τ measures the rate of change of the particle local distribution relaxing to equilibrium state. We replaced eqs. (6-10) in eq. (1), and it is obtained at order ε:

$$-\frac{f^{1}{}_{i,j}}{\tau} = \delta t(\frac{\partial}{\partial t_1} + \vec{e} \cdot \nabla) f^{0}{}_{i,j} \quad (18)$$

At order $\mathcal{E}^2$:

$$-\frac{f^{2}{}_{i,j}}{\tau} = \delta t(\frac{\partial}{\partial t_1} + \vec{e} \cdot \nabla) f^{1}{}_{i,j} + \delta t^2 \left(\frac{\partial f^{0}{}_{i,j}}{\partial t_2} + (\frac{\partial}{\partial t_1} + \vec{e} \cdot \nabla)^2 f^{0}{}_{i,j} \right) \quad (19)$$

Replacing eq. (18) in eq. (19) and using definitions eqs. (12-13), we obtain:

With

$$\frac{\partial \rho_j}{\partial t} + \nabla \cdot \vec{u}_j = 0 \quad (20)$$

$$\frac{\partial \vec{u}_j}{\partial t} + \nabla \cdot \Pi_j = 0 \quad (21)$$

With

$$\prod_{\alpha,\beta} = \sum_i \vec{e}_{i,\alpha} \vec{e}_{i,\beta} (f^{eq}{}_{i,j} + (1 - \frac{1}{\tau}) f^{1}{}_{i,j}) \quad (22)$$

And $\vec{e}_{i,\alpha}$ is the vector velocity component in α direction. We use the D2Q9 velocity scheme shown in Fig. 1, [3]. The weights w_i in the directions of each cell velocity point are:

$$w_i = \begin{Bmatrix} \frac{4}{9} & \rightarrow & i = 0 \\ \frac{1}{9} & \rightarrow & i = 1,2,3,4 \\ \frac{1}{36} & \rightarrow & i = 5,6,7,8 \end{Bmatrix} \quad (23)$$

Addresses $\vec{e}_{i,\alpha}$ and weights w_i satisfy the following tensorial relationships:

$$\sum w_i e_{i,\alpha} = 0 \quad (24)$$

$$\sum w_i e_{i,\alpha} e_{i,\beta} = \frac{1}{3} \delta_{\alpha,\beta} \quad (25)$$

$$\sum w_i e_{i,\alpha} e_{i,\beta} e_{i,\gamma} = 0 \quad (26)$$

The general form of the equilibrium distribution function is given by, [3]:

$$f^{eq}{}_{i,j} = \rho(a + b\vec{e}_i \cdot \vec{u} + c(\vec{e}_i \cdot \vec{u})^2 + d(\vec{u})^2) \quad (27)$$

Where a, b, c and d are lattice constants. Using equations (20), (21) and (eq22) we can show that eq. (27) is:

$$f^{eq}{}_{i,j} = \rho(1 + 3\vec{e}_i \cdot \vec{u} + \frac{9}{2}(\vec{e}_i \cdot \vec{u})^2 - \frac{3}{2}(\vec{u})^2) \quad (28)$$

Replacing eq. (28) in eq. (22), we obtain:

$$\prod^{0}{}_{\alpha,\beta} = \sum_i \vec{e}_{i,\alpha} \vec{e}_{i,\beta} (f^{eq}{}_{i,j}) = p\delta_{\alpha,\beta} + \rho u_\alpha u_\beta \quad (29)$$

And

$$\prod^{1}{}_{\alpha,\beta} = (1 - \frac{1}{2\tau}) \sum_i \vec{e}_{i,\alpha} \vec{e}_{i,\beta} (f^{eq}{}_{i,j}) = \nu(\nabla_\alpha(\rho u_\beta) + \nabla_\beta(\rho u_\alpha)) \quad (30)$$

Where $\nu = (1 - \frac{1}{2\tau})/6$ is defined as the viscosity and we have assumed the state equation to be $p = \rho/3$. Therefore, the momentum equation is, [3]:

$$\rho(\frac{\partial u_\alpha}{\partial t} + \nabla_\beta(u_\alpha u_\beta) = -\nabla_\alpha p + \nu \nabla_\beta \cdot (\nabla_\alpha(\rho u_\beta) + \nabla_\beta(\rho u_\alpha)) \quad (31)$$

3. Model of several fluids and potential interaction between particles

For a system consisting of several fluids [2], we suppose that each one of them obeys a distribution function given by eq. (28), with a temporal evolution on a D2Q9 lattice velocity. Furthermore, the total density of the system is taken as an average over the individual densities, weighted by the rates of change ω_1 and ω_2 for the two fluids, which measure the approach to equilibrium. Therefore:

$$\rho_{Total} = \rho_1\omega_1 + \rho_2\omega_2 \quad (32)$$

Similarly, the components of the overall speed of the system are taken as a weighted average given by ω_1 and ω_2, in the same manner as was done with ρ_{Total}, so:

$$u_{Total,x} = \frac{j_{1,x}\omega_1 + j_{2,x}\omega_2}{\rho_{Total}} \quad (33)$$

$$u_{Total,y} = \frac{j_{1,y}\omega_1 + j_{2,y}\omega_2}{\rho_{Total}} \quad (34)$$

On the other hand, for each of the fluids, it is assumed on the grid point that a change of momentum is given by a repulsive potential, which interacts with its nearest neighbors, and it is defined by, [2], [21] and [22]:

$$V(\vec{r},\vec{r}') = \sigma_{\vec{r},\vec{r}'}\psi(\vec{r})\psi(\vec{r}') \quad (35)$$

Where $|\sigma_{\vec{r},\vec{r}'}|$ is a Green function $\psi(\vec{r})$ and $\psi(\vec{r}')$, are effective density distribution functions. Now, in view of the fact that we only consider interactions with nearest neighbors, we define the Green function as:

$$\sigma|\vec{r}-\vec{r}'|_{i,i'} = \begin{Bmatrix} 0 & if & |\vec{r}-\vec{r}'|>0 \\ |\sigma_{i,i'}| & if & |\vec{r}-\vec{r}'|=0 \end{Bmatrix} \quad (36)$$

Where $|\sigma_{i,i'}|$ defines the weight of the interaction between the two systems and the sign determines whether the potential is attractive or repulsive. Therefore, the induced moment on the grid point is:

$$\frac{\partial \vec{P}_i}{\partial t} = \psi(\vec{r})\sum_{i'}\sigma_{i,i'}\psi(\vec{r}+\vec{e}) \quad (37)$$

Therefore, the momentum after the collision is:

$$\frac{\partial \rho\vec{u}_i}{\partial t} = \frac{\partial \rho\vec{u}}{\partial t} + \tau\frac{\partial \vec{P}_i}{\partial t} \quad (38)$$

Given this model, we have made simulations and their results will be present in section 5.

4. Experimental setup

The periodic consists of p-type silicon (boron doped, single crystalline orientation [111]) polished wafers with 525 micron thickness and 0.01 to 0.02 Ωm resistance. Samples were prepared according to published experimental details in reference [23].

The manufactured surfaces were determined using a ZEISS M700 laser confocal microscope and a Cary 5000 UV-VIS-NIR spectrophotometer. With the help of its analytical software the 3D areal surface texture is identified.

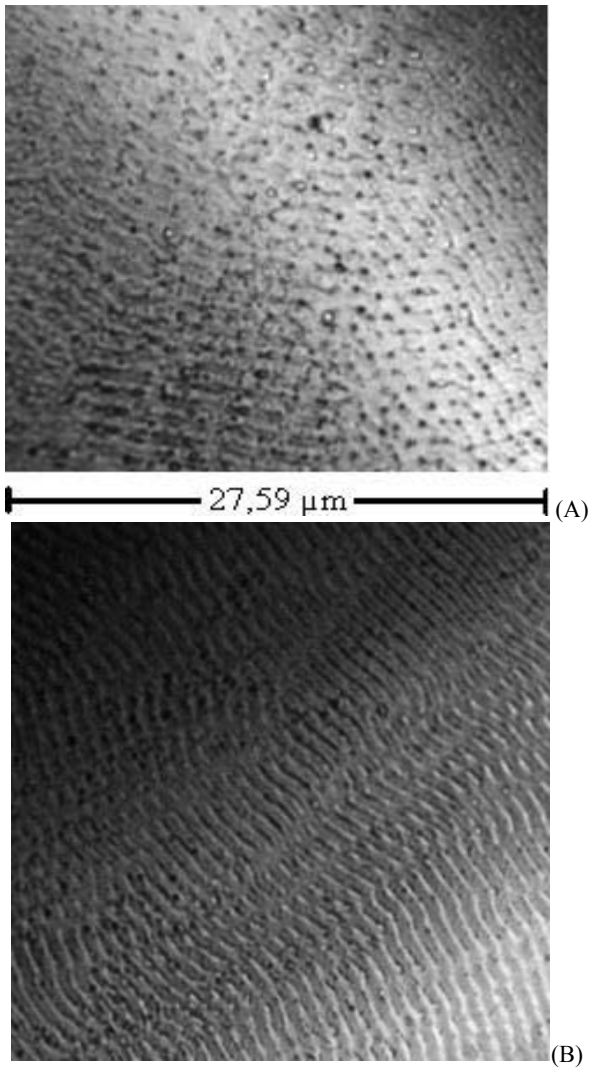

Figure 2. Samples irradiated with 620 J. (A)- without gas and (B)- with Ar gas, [31]. Figures obtained using a confocal laser microscope.

In the current literature, the formation of the periodic structures has been explained as being due to the polarization of the laser and the scanning of the sample by the laser [24], which impedes the interaction between the laser and the plasma (produced by evaporated material). Under our experimental conditions, we obtained incipient periodic structures without blowing gas, (Fig. 2 A), and with the gas, the formation of periodic structures is improved, due to the evacuation of the evaporated material, which has the same effect as the scanning of the sample with the laser figure (Fig. 2 B).

In Figs. 3 A-F, we show the experimental results. figures A-B were produced at the threshold energy range 465 J for a periodic well-defined structure formation. Surfaces Figs. 3 C-D show sharp structures, but with some non-removed areas, perhaps, due to the gas low efficiency of removal of ablated material during laser irradiation. Figs. 3 E-F show a sample handled with 3100 J that almost shows the spatial periodicity structure, suggesting an optimal energy level (i.e. 620 J) for generating clear periodic structures.

The formation of a periodic structure through the

simultaneous incidence of the three laser lines on the surface of silicon is due to the energy supplied by the three wavelengths, which increases the surface temperature of silicon to 1613 K. At this temperature, the melting point of silicon is reached. This allows the formation of a non-ideal fluid, which generates the periodic structure once the surface sample is solidified. Based on this hypothesis, we constructed a computer simulation that reproduces the experimental pattern, which is discussed later.

Moreover, experimental results show that there is an energy threshold for the formation of the periodic structure. This energy threshold can be defined as the energy required for melting the silicon surface enough to obtain a periodic structure. In our study, this energy is found to be 620J.

The importance of using the laser lines to produce periodic structure lies in the fact that electro-mechanical systems are not necessary in order to scan the sample with the laser, nor are optical devices (beam splitters, focal lenses, mirrors and beam expanders) [25-26]. Furthermore, the mean square depth (500-700nm) of the periodic structure fabricated with the laser lines is higher than those reported for periodic structures formed with one only laser line (10-30nm) [27]. This difference is important for the development of optical devices such as optic filters and pass-bands.

5. Simulation Results

In order to explain the patterns seen in Figs. 2 and. 3, which show experimental results, we proposed a two non-miscible non-ideal fluid system. We assume that the line component of the incident laser 355 nm, the most energetic one, and the 532 nm close to the experimental average distance between peaks 547 ± 13 nm, [23] on the surface, cause a melting of material, becoming two non-ideal interacting fluids. The third, the lowest energy, is transparent for the system. Basically, the action of the laser on the silicon surface creates a two fluid phase, resulting in a final state given by the patterns.

We did simulations with a system size of 186x186, for a simulation time of 200, and assuming an initial random distribution for the distribution function. The left panel in Fig. 4 shows the simulation result based on the Lattice-Boltzmann simulation result for the density, ρ, of the system, and the right one exhibits the confocal microscope images result. Clearly, the simulation results show the formation of parallel oblique long stripes, or ripples, which are the fundamental geometric structure of the experimental patterns, and they are shown in the right panel of Fig. 4.

It is possible to explain the pattern formation as being produced by the excited electrons in the band structure generating the crystalline disorder at the surface. However, as long as the energy flux on surface persists, the long range order holds, avoiding reaching the statistical equilibrium. Therefore, this instability, out of equilibrium, can be considered as the interplay between surface roughening and surface smoothing [28].

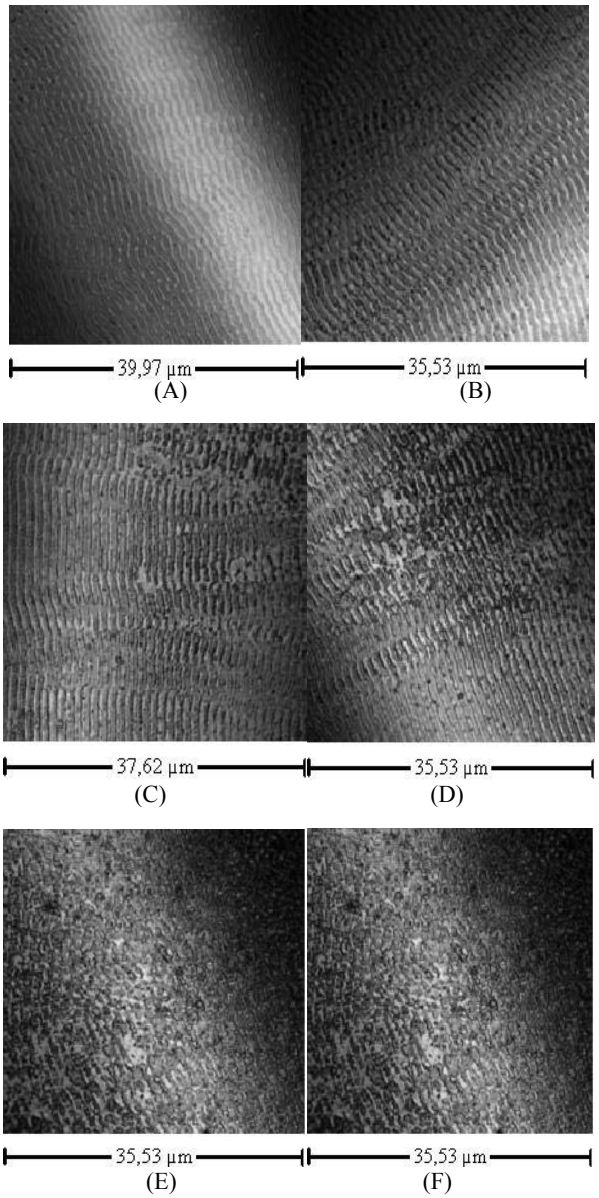

Figure 3. Confocal microscope images of samples irradiated with different amounts of energy and argon gas blowing, [23], [31]. Figures obtained using a confocal laser microscope.

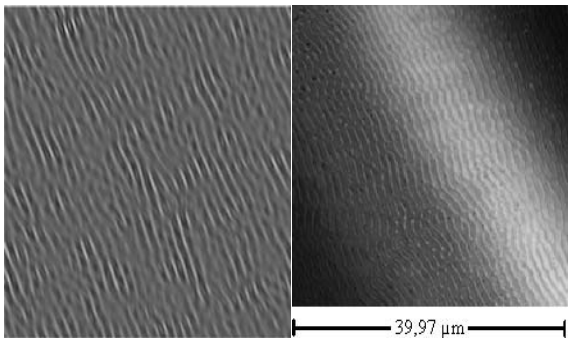

Figure 4. Comparison between simulation for a 186x186 lattice size using a Lattice-Boltzmann simulation, left panel, and experimental result, right panel. Simulation result elaborated in gnuplot [32], and right figure obtained using a confocal laser microscope.

These two physical effects can be modeled using some type of Cahn-Hilliard/Kuramoto-Sivashinsky differential equation (CHKS) [29-31], which constitutes a mean field approach to problems at the mesoscopic level, and offers pattern structures such as stripes, squares etc. This theoretical approach is also shared by Lattice-Boltzmann [3], and for this reason the simulation is able to reach a possible result offered by a CHKS procedure.

6. Conclusions

Using the hypothesis of a two non-ideal fluids interaction governed by lattice Boltzmann method, we can reproduce quite well the periodic parallel diagonal stripes structures found experimentally with the use of a nanosecond multiline Nd:YAG laser on a single-crystalline silicon.

Acknowledgments

We gratefully acknowledge the support of the Bogotá Research Division of the National University of Colombia under the grants DIB-7178, DIB-90201022 and DIB-8003355.

References

[1] Qian, Y. H., d'Humières, D. and Lallemand, P., Lattice BGK models for Navier-Stokes equations., Europhysics Letters, 17 (6), pp. 479-484. 1992.

[2] Shan, X. and Chen, H., Lattice Boltzmann model for simulating flows with multiple phases and components., Physical Review E, 47 (3), pp. 1815-1820, 1993.

[3] Wolf-Gladrow, D.A., Lattice-Gas cellular automata and Lattice Boltzmann Models, an Introduction, Springer-Verlag, Berlin Heidelberg, 2000.

[4] Bathnagar, P.L., Gross, E.P. and Krook, M., A model for collision processes in gases. I. Small amplitude processes in charged and neutral one-component systems., Phys. Rev. 94, pp. 511-525, 1954.

[5] Dellar, P.J., Lattice kinetic formulation for ferrofluids, J. Statist. Phys., 121, pp. 105-118, 2005.

[6] Sofonea, V. and Früh, W.G., Lattice Boltzmann model for magnetic fluid interfaces, Eur. Phys. J., B 20, pp. 141-149, 2001.

[7] Wang, M., Pan, N., Wang, J. and Chen, S., Lattice Poisson-Boltzmann simulations of electroosmotic flows in charged anisotropic porous media, Communications in Computational Physics, 2 (6), pp. 1055-1070, 2007.

[8] Zhang, J. and Yan G., A lattice Boltzmann model for the Korteweg-de Vries equation with two conservation laws. Computer Physics Communications, 180 (7), pp. 1054-1062, 2009.

[9] Dellar, P.J., Lattice kinetic schemes for magnetohydrodynamics, Journal of Computational Physics, 179, pp. 95-126, 2002.

[10] Palpacelli, S. and Succi, S., The quantum Lattice Boltzmann equation: recent developments, Communications in Computational Physics, 4 (5), pp. 980-1007, 2008.

[11] Yiotis. A.G., Psihogios, J., Kainourgiakis, M.E., Papaioannou, A. and Stubos, A.K., A lattice-Boltzmann study of viscous coupling effects in immiscible two-phase flow in porous media. Colloids and Surfaces A: Physicochem. Eng. Aspects, 300, pp. 35-49, 2007.

[12] Luo, L.S. and Girimaji, S.S., Theory of the lattice Boltzmann method: Two-fluid model for binary mixtures, Physical Review E, 67, 036302 2003.

[13] Vorobyev, A.Y. and Guo, C., Spectral and polarization responses of femtosecond laser-induced periodic surface structures on metals, C. Journal of Applied Physics, 103 (4), p 043513-1. 2008.

[14] Trtica, M., Gakovic, B., Radak, B., Batani, D., Desai, T. and Bussoli, M., Periodic surface structures on crystalline silicon created by 532 nm picosecond Nd:YAG laser pulses, Applied Surface Science, 254, pp. 1377-1381, 2007.

[15] Feng, Z.C. and Tsu, R., Eds., Porous Silicon, World Scientific, Singapore, 41 P., 1994.

[16] Bisi, O., Ossicini, S. and Pavesi, L., Porous silicon: A quantum sponge structure for silicon based optoelectronics, Surface Science Reports, 38 (1), pp. 1-126, 2000.

[17] Zhao, X., Schoenfeld, O., Nomura, S., Komuro, S., Aoyagi, Y. and Sugano, T., Nanocrystalline Si: A material constructed by Si quantum dots, Materials Science and Engineering B, 35 (1), pp. 467-471, 1995.

[18] Ramírez, A., Fonseca, L.F. and Resto, O., Estimation of Silicon Nanocrystalline Sizes from Photoluminescence Measurements of RF Co-Sputtered Si/SiO2 Films, Materials Research Society Symposium Proceedings. 737, F3.30.1, 2003.

[19] Dickey, M., Holswade, C. and Shealy, L., Laser beam shaping applications, Taylor & Francis-CRC Press, 2006.

[20] Misawa, H. and Juodkazis, S., 3D laser microfabrication principles and applications, Wiley-Verlag, Weinheim, 2006.

[21] Shan, X. and Chen, H., Lattice Boltzmann model for simulating flows with multiple phases and components, Phys. Rev. E, 47 (3), pp. 1815-1819, 1993.

[22] Yuang, P. y Schaefer, L., Equations of state in a lattice Boltzmann model, Phys. of Fluids 18, pp. 042101-1 - 042101-11, 2006.

[23] Alfonso-Orjuela, J.E., Andrade-Zambrano, D.F. and Arroyo-Osorio, J. M., Refractive index of multiline nanosecond laser-induced periodic surface structures and porous silicon, Revista Mexicana de Física, 57, pp 475 - 480. 2011.

[24] Sano, T., Yanai, M., Ohmura, E., Nomura, Y., Miyamoto, I., Hirose, A., and Kobayashi, K., Femtosecond laser fabrication of microspike-arrays on tungsten surface, Applied Surface Science, 247, pp. 340 – 346, 2005.

[25] Al-Naimee, K.A., Nanostructure formation in Silicon photovoltaic cell surface by femtosecond laser pulses, Indian Journal of Science and Technology, 3 (3), pp. 308 -310, 2010.

[26] Horita, S., Kaki, H. and Nishioka, K., Surface modification of an amorphous Si thin film crystallized by a linearly polarized Nd:YAG pulse laser beam, Journal of Applied Physics, 102 (1), pp. 013501-1 - 013501-10, 2007.

[27] Boghosian, B.M., Chow, C.C. and Hwa, T., Hydrodynamics of the Kuramoto–Sivashinsky equation in two dimensions, Phys. Rev. Lett. 83, pp. 52-62. 1999.

[28] Kuramoto, Y., Chemical oscillations, waves, and turbulence, Springer-Verlag, Berlin, Heidelberg, 1984.

[29] Cahn, J.W. and Hilliard, J.E., Free energy of a nonuniform system. I. Interfacial free energy, J. Chem. Phys. 28, pp. 258-267, 1958.

[30] Garzón-Alvarado, D., Galeano, C. and Mantilla, J., Pruebas numéricas sobre la formación de patrones en medios heterogéneos 2d: Una aproximación a través del modelo Schnakenberg, DYNA, 79. (172), pp. 56-66. 2012.

[31] Andrade, D., Fabricación de redes de difracción sobre silicio monocristalino con láser pulsado multilinea de Nd YAG, MSc. Tesis, Universidad Nacional Colombia, Bogotá Colombia, 2012.

[32] Gnuplot 4.6.0: An interactive plotting program, august 2012. http://www.gnuplot.info

F. R. Fonseca-Fonseca, received the Physics degree in 1993, the MSc. in Physics Science in 1998, both from the Universidad Nacional de Colombia and the PhD degree in Physics in 2004. From 1994 to 1999, he worked in basics aspects of quantum field theory applied to gravity theory and quantum field theory at finite temperature. Also, he has worked in statistical systems outside of the equilibrium. Currently, he is associated Professor in the Physics Department, Facultad de Ciencias, Universidad Nacional de Colombia and belongs to the group of Surfaces and Materials Science at the same university. His research interests include: simulation, modeling and in particular the use of Lattice-Boltzmann technique applied to solve complex systems.

J. E. Alfonso-Orjuela, received the Bs. degree in Physics in 1987 and his MSc. degree in Science - Physics in 1991, both of them being obtained from the Universidad Nacional de Colombia. In 1997 he completed his PhD. in Science -Physics at the Universidad Autonoma de Madrid, Spain.

He has been linked to the Universidad Nacional de Colombia as a full professor since 2000, he belongs to the Group of Materials Science and Surface and he is an associate researcher at the International Centre of Physics (CIF) at the same university. His research has been focused on material science, particularly on thin film processing as well as performance characterization, studying thin film optical, electrical and mechanical properties.

D. F. Andrade, completed his Bs. degree in Physics-Engineering in 2008, from Universidad del Cauca, Colombia and his MSc. degree in Science Materials Engineering in 2012 from the Universidad Nacional de Colombia. He has been linked to the Universidad Gran Colombia as a full professor since 2013, he also belongs to Group Surfaces and Materials Science to the Universidad Nacional de Colombia, where his research has been focused on material science.